ChemistrySelect

Research Article
doi.org/10.1002/slct.202403782

Chemistry Europe
European Chemical Societies Publishing

www.chemistryselect.org

Thermal Stability and Electrical Conductivity of Polyvinyl Alcohol Composites Reinforced with Mn_2O_3–rGO

R. Gamal,[a] T. S. Soliman,*[b] and A. Khalid[c, d]

The current work is concerned with the study and examination of the thermal and electrical characteristics of polyvinyl alcohol (PVA)/Mn_2O_3–reduced graphene oxide (rGO) nanocomposite. The Mn_2O_3–rGO composite was synthesized using a hydrothermal approach technique, and then PVA films were strengthened with varying amounts of Mn_2O_3–rGO nanoparticles (NP) prepared by the casting method. Raman analysis was applied to polymer films to ensure the complexation between the PVA and Mn_2O_3–rGO. Thermogravimetric analysis (TGA) and electrical analysis are used to investigate the effect of Mn_2O_3–rGO NP on the thermal stability and electrical conductivity of the polymer films. The films' thermal stability was raised by increasing the Mn_2O_3–rGO content in the PVA matrix. The polymer films exhibit an increase in electrical conductivity from 2.023×10^{-8} S·cm^{-1} for pure PVA to 1.895×10^{-5} S·cm^{-1} for PVA-1.5% Mn_2O_3–rGO, which arises from the rise in free charge carrier mobility and hopping ionic hopping. Furthermore, in accordance with the Arrhenius relation, conductivity increases with temperature. The results nominated the present composite in flexible electronic applications.

1. Introduction

Introducing nanoparticles to a polymer matrix is one of the common methods for producing new materials with enhanced physical properties in modern science and technology.[1,2] This field of work is in progress for replacing the hard metals with a flexible organic material.[3] So, most of the researcher's work is in the direction of enhancing polymer materials more and more through the use of different types of metal oxides.[1,3,4] Early on, a lot of work has been done on enhancing the physical properties of the polyvinyl alcohol (PVA) matrix through reinforcing metal oxides. PVA was selected because of its good characteristics, which include high capacity, good film formation, and good dielectric properties. Several metal oxides, like CuO,[4] ZnO,[3] SiO_2,[5] TiO_2,[6] Fe_3O_4,[7] MgO,[8] and others, were reinforced in PVA, and fascinating results were obtained. Furthermore, researchers have found that adding graphene oxide to the PVA matrix separately or as a composite with metal oxides can enhance the thermal and conductivity of the matrix.[9,10]

Graphene exhibits a high degree of charge carriers mobility, high transport efficiency, a large surface area, excellent electrical conductivity, ultrahigh mechanical properties, and excellent chemical stability.[2,11,12] These ideal properties make it appropriate for several applications like sensors, batteries, and catalysts, but reduced graphene oxide (rGO) is very useful in the production of large-scale graphene-based materials.[13–15] Several reports have recently been done using rGO and/or GO sheets inside the polymer matrix that enhanced their structural and physical properties.[16–18] Several metal oxides, like Fe_3O_4,[19] Co_3O_4,[20] CoO-Li_2O,[21] ZnO-NiO,[22] Mn_2O_3-rGO,[23,24] SnO_2,[25] and MnO[26] have a wide range of uses in various fields, such as the application of radiation resistance, storage devices, semiconductor transistors, etc. Manganese oxide (Mn_2O_3) is highly stable, low-cost, and environmentally friendly when compared to other metal oxides, particularly in energy storage applications where it exhibits excellent catalytic efficiency and a large surface area. Combining Mn_2O_3 and rGO has been shown to be extremely beneficial for creating nanocomposites with great electrochemical efficiency.[11,23,24,27]

The Mn_2O_3–rGO nanoparticles were first synthesized and then inserted into the PVA matrix at various concentrations. XRD, surface roughness, and UV–visible investigations have previously been investigated.[28] Herein, the Raman shift, thermal, and electrical properties have been investigated. The thermal and electrical characteristics of PVA-Mn_2O_3/rGO films were studied via a thermogravimetric analyzer (TGA) and CHI604E electrochemical workstations.

2. Experimental Section and Methods

Polyvinyl alcohol (PVA) films doped with varying amounts of Mn_2O_3–rGO were synthesized as described previously,[28] and the process is illustrated in the schematic synthesis shown in Figure 1. The Mn_2O_3–rGO composite was prepared via the hydrothermal method,[24] 0.6 g Mn_2O_3 and 0.3 g GO (ratio 2:1) were dissolved in 100 mL distilled water and sonicated for 15 min. Then, the as-prepared Mn_2O_3–rGO composite was added

[a] R. Gamal
Elsewedy University of Technology-Polytechnic Egypt, Egypt

[b] T. S. Soliman
Institute of Natural Sciences and Mathematics, Ural Federal University, Ekaterinburg 620000, Russia
E-mail: tarek.attia@fsc.bu.edu.eg

[c] A. Khalid
Department of Basic Engineering Sciences, Faculty of Engineering at Shoubra, Benha University, Cairo, Egypt

[d] A. Khalid
Higher institute for Optics Technology, Cairo, Egypt

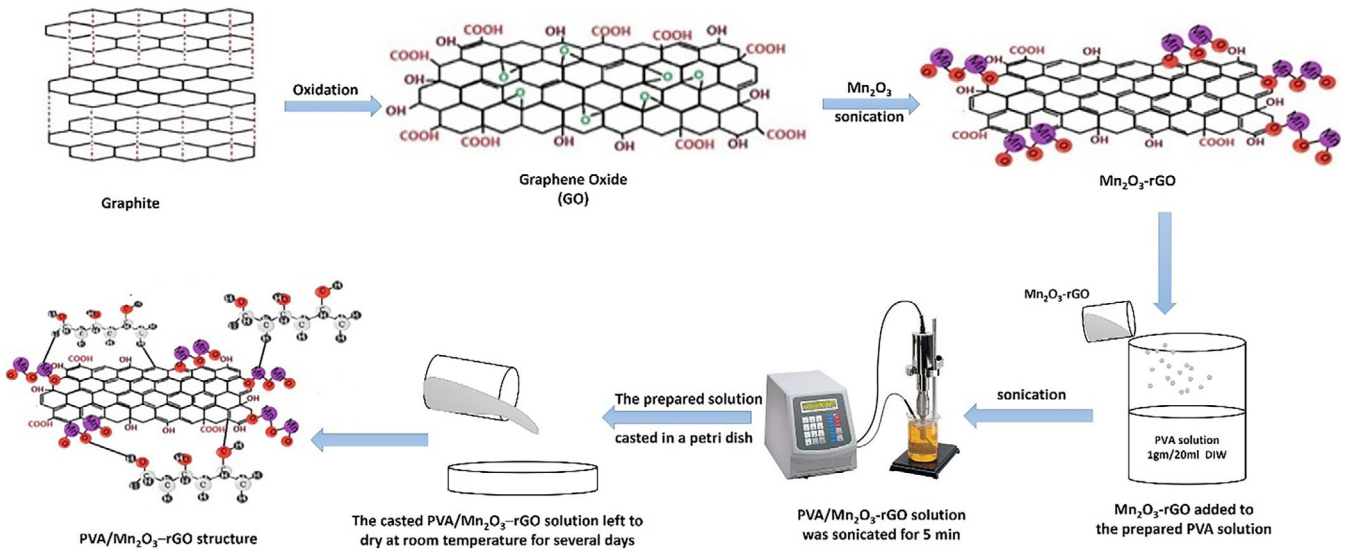

Figure 1. Schematic steps of PVA/Mn_2O_3–rGO film synthesis.

to the PVA solution (1 g PVA/20 mL distilled water) with different concentrations and distributed using the probe ultrasonic procedure. The mixed solutions were poured into glass dishes and left to dry in a warm atmosphere for several days. The PVA/Mn_2O_3–rGO films are labelled as pure PVA, M_1, M_2, M_3, and M_4 for 0, 0.5, 1.0, 1.5, and 2.0% Mn_2O_3–rGO, respectively. Thermal analyses (TGA) were measured by Themsus One+, SETARAM, France, N_2 atmosphere, and heats from 30 °C to 900 °C, with a temperature rate of 10 °C/min. The CHI604 electrochemical workstation model was used to study electrochemical impedance spectroscopy (EIS). ZView software was employed for the analysis of the acquired data. Using EIS, the ionic conductivities of the samples were determined at various temperatures (308–338 K) in the 10–10^6 Hz frequency range.

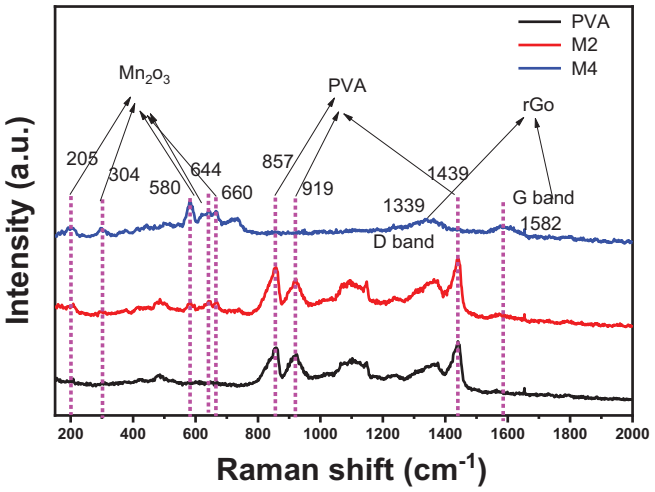

Figure 2. Raman shifts of the PVA/Mn_2O_3–rGO films.

3. Results and Discussion

3.1. Raman Analysis

Raman spectroscopy is an essential analytical tool for characterizing materials and provides insights into their molecular composition and structural properties. The data was recorded using a laser with an excitation wavelength of 633 nm. The Raman shifts for pure PVA, M_2, and M_4 films are represented in Figure 2.

The Raman spectra display distinct peaks at 857 (C—C strech), 919 (C—C strech), and 1439 (C—H and O—H bend) cm^{-1} for the PVA thin film.[29] By adding 1% (M_1) and 2% (M_2) of Mn_2O_3–rGO nanocomposite to the PVA film, additional peaks are observed at 205, 304, 580, 644, and 660 cm^{-1}. These peaks are the distinctive for Mn_2O_3, which agreed well with the literature.[30–33] Moreover, additional characteristic peaks at 1339 (D band) and 1582 cm^{-1} (G band) are characteristic of rGO as reported in the literature.[24,34,35] As the concentration of Mn_2O_3-rGO increases, the intensity of the distinct peaks of pure PVA decreases, while the intensity of the peaks associated with the Mn_2O_3 rises. This can be associated with the formation of hydrogen bonding between the functional group of Mn_2O_3–rGO and the PVA. Furthermore, the intensity of G and D bands is increased for the M2 sample compared to the pure PVA, indicating the increase of the disordering in the polymer matrix.[24,34,35] This result matched the XRD data in previous work.[28] The D and G bands lessened at higher concentrations (M4 sample) can be ascribed to the higher content of Mn_2O_3 and the agglomerations that may cover the Raman signal from both G and D, reducing their intensity. This result indicates a good interaction between Mn_2O_3–rGO and PVA.

3.2. Thermal Analysis

Thermal stability is crucial in determining a polymer's ability to maintain functionality at elevated temperatures. The ther-

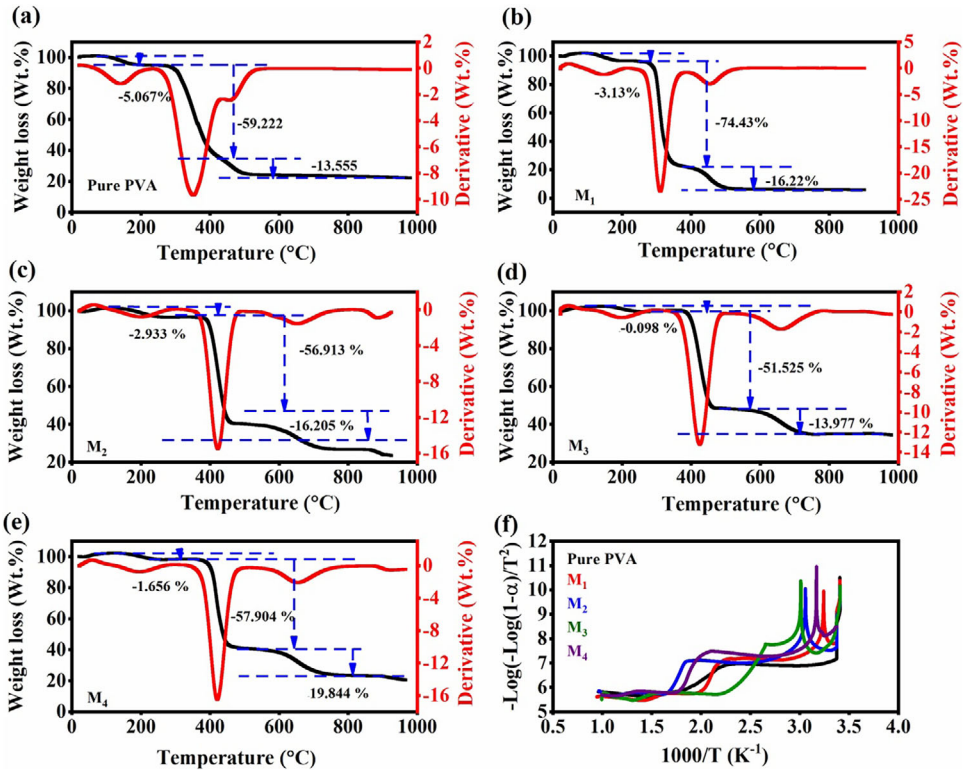

Figure 3. (a–e) TGA and DTGA curves of the PVA/Mn_2O_3-rGO films and (f) -log[-log(1-α)/T^2] versus 1000/T for PVA/Mn_2O_3–rGO films.

mogravimetric analysis (TGA) and differential thermogravimetric analysis (DTGA) curves of PVA/Mn_2O_3–rGO films are presented in (Figure 3a–e). Adding Mn_2O_3–rGO significantly enhances the thermal stability of the polymer films, with three distinct stages of weight loss observed. In the initial stage, the weight loss is primarily attributed to the evaporation of physiosorbed water from the sample.[36,37] The second stage of weight loss is associated with the decomposition of hydroxyl and carboxyl groups within the reduced graphene oxide (rGO), with the complete decomposition of rGO occurring around 600 °C.[27] The third stage involves the degradation of the polymer matrix, which is linked to the carbonization and collapse of the polymer chains. The degradation temperature in this phase was further confirmed using DTGA.[37,38] The thermal activation energy (E) of the films was calculated using the Coates and Redfern equation:[39]

$$log\left[\frac{-log(1-\alpha)}{T^2}\right] = log\frac{R}{\Delta E}\left[1-\frac{2RT}{E}\right]-\frac{E}{2.304RT} \quad (1)$$

where T is the temperature in Kelvin, R is the universal gas constant (8.31 J/mol K), and α is a weight ratio obtained by the following equation:

$$\alpha = \frac{\omega_i - \omega_t}{\omega_{i-\omega_f}} \quad (2)$$

where w_t is the actual weight, w_i is the initial weight and w_f is the sample final weight. Plotting –log[-log(1-α)/T^2] versus 1000/T helps to determine the E value using the equation:

$$E = 2.303R \times slope \quad (3)$$

By plotting -log[-log(1-α)/T^2] against 1000/T, the activation energy (E) can be determined from the slope of the resulting curve, as illustrated in Figure 3f. The values of activation energy for the different stages of the PVA/Mn_2O_3–rGO films are provided in Table 1. These results demonstrate that energy activation generally increases with higher Mn_2O_3–rGO content, suggesting enhanced thermal stability.

Table 1. Thermal parameters of PVA/Mn_2O_3–rGO films.

Sample	Activation Energy (Region I)	Activation Energy (Region II)	Activation Energy (Region III)
Pure PVA	0.61	40.32	5.33
M_1	15.23	58.46	1.81
M_2	11.83	65.37	3.85
M_3	2.23	20.99	2.58
M_4	12.25	81.98	7.85

3.3. Ac Conductivity Properties

The cole–cole plot of PVA and PVA/Mn_2O_3–rGO films is presented in Figure 4a. The plot does not exhibit a perfect semicircular shape, but still allows for the calculation of the bulk resistance (R_b). It was observed that R_b decreases with an increase in the Mn_2O_3–rGO concentration within the PVA matrix. The intercept on the Z'-axis can be used to calculate both the bulk-resistance (R_b) and the bulk-conductivity (σ_b) (Table 2) as follows:[40]

$$\sigma_b = \frac{1}{R_b} \times \frac{t}{A} \quad (4)$$

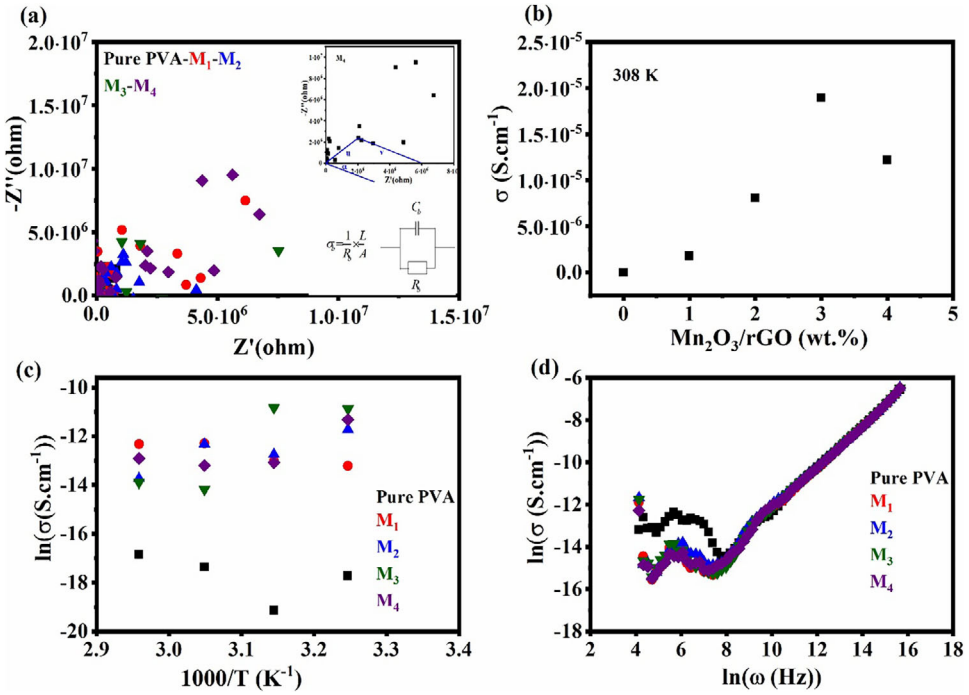

Figure 4. (a) Col–col plots. (b) The bulk conductivity of the Mn_2O_3–rGO content in PVA. (c) The conductivity versus the temperature. (d) The conductivity versus the frequency for PVA/Mn_2O_3-rGO films.

Table 2. The activation energy (E_a) and relaxation time (τ) of PVA/Mn_2O_3-rGO films.

Samples	R_b (Ω)	σ_b ($S.cm^{-1}$)	E_a I (eV)	E_a II (eV)	τ (s)	s
Pure PVA	1,007,402	2.02×10^{-8}	1.18	1.05	7.18×10^{-4}	0.60
M_1	9070	1.83×10^{-6}	0.18	0.32	6.05×10^{-4}	0.77
M_2	2043	8.11×10^{-6}	0.84	0.44	1.33×10^{-4}	0.75
M_3	874	1.89×10^{-5}	0.04	0.14	6.08×10^{-4}	0.76
M_4	1358	1.22×10^{-5}	1.46	0.75	4.41×10^{-5}	0.78

where t is the thickness of the polymer films and A is the area of the surface. Figure 4b shows the relationship between bulk conductivity (σ_b) and the concentration of Mn_2O_3–rGO in the PVA matrix. As the concentration of Mn_2O_3–rGO increases, the conductivity rises, reaching a value of 1.9×10^{-5} Scm^{-1} for the M3 sample. This increase in conductivity is attributed to the high porosity and large surface area of the Mn_2O_3–rGO, which enhances charge transfer within the polymer matrix.[41,42]

Figure 4c displays the plot of $L_n(\sigma)$ versus 1000/T from 308 K to 338 K for all the polymer films. The data follows the Arrhenius relation:[8,43]

$$\sigma = \sigma_o \; e^{\left(-\frac{E_a}{KT}\right)} \tag{5}$$

where σ is the conductivity at temperature T, and σ_o, K, and E_a are, respectively, constant, the Boltzmann constant, and the activation energy. As shown in Figure 4c, the conductivity increases as the temperature increases, which is attributed to the free volume model. This model suggests that as the temperature increases, the free volume also increases, facilitating polymer expansion, enhancing charge transfer, and increasing conductivity.[8] Two distinct regions are observed: from 3.25 to 3.1 K^{-1} and from 3.14 to 2.96 K^{-1}, indicating different conduction mechanisms and material behaviors at low and high temperatures (Table 2). These two temperature ranges are below the PVA glass transition temperature (T_g = 343 K), suggesting that the conductivity mechanisms are active in the temperature region below the T_g.[44] When doping the PVA with Mn_2O_3–rGO, the activation energy E_a is notably lower than 0.8 eV, indicating that charge transport occurs via electron motion at lower temperatures, below the T_g, consistent with Jonscher's theory of electronic conduction.[44,45] As the temperature increases, PVA undergoes expansion, increasing the free volume, allowing greater electron mobility, and further enhancing thebrk conductivity.[46]

Figure 4d presents the conductivity of pure PVA and PVA/Mn_2O_3–rGO films as a function of frequency at 308 K. The conductivity of films increases with increasing frequency. This frequency-dependent behavior of the conductivity follows the universal power law:[47,48]

$$\sigma_{tot}(\omega) = \sigma_{dc} + A\omega^s \tag{6}$$

where σ_{dc} is the dc conductivity, A is constant, ω is the angular frequency of the electric field, and s is the exponent factor which obtained by using the least square fitting of Equation (6). The values of the exponent factor s are presented in Table 2, suggesting that the conduction mechanism is governed by hopping conduction.[40,41,43] According to the jump relaxation model, at low frequencies, electrons hop from one site to another. At higher frequencies, due to shorter time intervals, the electrons can return to their origi-

nal sites more quickly, thus enhancing the overall conductivity. The relaxation time (τ) can be calculated using the following equation:[48]

$$\frac{v}{u} = (\omega\tau)^{1-h} \quad (7)$$

where v is the distance on the col–col plot between (O, R_b) and an experimental point, u is the distance between the experimental point and (0, 0) and $h = 2\alpha/\pi$ where α is the depressed angle from the Z'-axis (inset Figure 4a). Table 2 shows that the addition of Mn_2O_3–rGO to the PVA matrix leads to a reduction in τ. This is attributed to the increased free volume and enhanced conduction pathways, which facilitate the movement of electrons and polymer segments within the matrix, thereby improving the overall conductivity.

4. Conclusion

Polymer nanocomposites of PVA/Mn_2O_3–rGO films were fabricated successfully via the casting method. Structural characterization through Raman spectroscopy confirmed the incorporation of Mn_2O_3–rGO into the PVA matrix, with distinct Mn_2O_3–rGO bands observed. Thermal stability analysis via TGA demonstrated a significant enhancement in the thermal properties of the PVA films upon the addition of Mn_2O_3–rGO nanoparticles. The electrical conductivity of the PVA film was improved with an increase in the Mn_2O_3–rGO content. Electrical conductivity measurements revealed a noticeable improvement in the conductivity of PVA film with the incorporation of Mn_2O_3–rGO. The bulk conductivity increased up to 1.895×10^{-5} S·cm^{-1} for PVA-1.5% Mn_2O_3–rGO, indicating a substantial enhancement in charge transport. The activation energy for conductivity in the PVA/Mn_2O_3–rGO films decreased as the Mn_2O_3–rGO content increased, suggesting that the conduction mechanism shifts towards easier electron mobility with the addition of Mn_2O_3–rGO nanoparticles. In conclusion, the PVA/Mn_2O_3–rGO films with enhanced thermal and electrical conductivity are suited for applications in flexible electronic devices.

Acknowledgements

Funding is not applicable. The authors have nothing to report.

Author Contributions

R. Gamal: Conceptualization, investigation, methodology, data curation, Writing — review & editing. **T.S. Soliman**: Conceptualization, formal analysis, investigation, methodology, data curation, writing — review & editing. **A. Khalid**: Conceptualization, formal analysis, data curation, Writing — review & editing.

Conflict of Interests

The authors declare no conflict of interest.

Data Availability Statement

The data that support the findings of this study are available from the corresponding author upon reasonable request.

Keywords: Electrical conductivity · Mn_2O_3–rGO · Polymer composite · PVA · TGA

[1] O. G. Abdullah, S. B. Aziz, M. A. Rasheed, *Results Phys.* **2016**, *6*, 1103–1108.
[2] Abid, P. S., S. S. Islam, P. Mishra, S. Ahmad, *Defect States and Quantum Efficiency, Sci. Rep.* **2018**, *8*. https://doi.org/10.1038/S41598-018-21686-2.
[3] A. Khlyustova, N. Sirotkin, A. Kraev, A. Agafonov, V. Titov, *J. Appl. Polym. Sci.* **2021**, *138*, 51174. https://doi.org/10.1002/APP.51174.
[4] S. Gandhi, R. H. H. Subramani, T. Ramakrishnan, A. Sivabalan, V. Dhanalakshmi, M. R. G. Nair, R. Anbarasan, *J. Mater. Sci.* **2010**, *45*, 1688–1694.
[5] B. Karthikeyan, S. Hariharan, A. Sasidharan, V. Gayathri, T. Arun, A. Akbari-Fakhrabadi, C. Madhumitha, *Opt. Mater. (Amst)* **2019**, *90*, 139–144.
[6] S. D. Praveena, V. Ravindrachary, R. F. Bhajantri, *Polym. Compos.* **2016**, *37*, 987–997.
[7] B. Salah, A. I. Ayesh, *Molecules* **2021**, *26*, 1–10.
[8] G. Mohammed, A. M. El Sayed, W. M. Morsi, *J. Phys. Chem. Solids.* **2018**, *115*, 238–247.
[9] A. Badawi, S. S. Alharthi, *Appl. Phys. A Mater. Sci. Process.* **2022**, *128*, 1–15.
[10] A. Badawi, Gaber Mersal, A. S. Abdallah, A. Shaltout, J. Boman, M. Alsawat, M. A. Amin, *J. Polym. Res.* **2021**, *1*, 270.
[11] R. M. Mahani, A. G. Darwish, A. M. Ghoneim, *J. Electron. Mater.* **2020**, *49*, 2130–2136.
[12] R. Lv, X. Wang, W. Lv, Y. Xu, Y. Ge, H. He, G. Li, X. Wu, X. Li, Q. Li, *J. Chem. Technol. Biotechnol.* **2015**, *90*, 550–558.
[13] Q. Xiang, J. Yu, M. Jaroniec, *J. Am. Chem. Soc.* **2012**, *134*, 6575–6578.
[14] H. Jiang, *Small* **2011**, *7*, 2413–2427.
[15] S. Yang, X. Feng, K. Müllen, *Adv. Mater.* **2011**, *23*, 3575–3579.
[16] S. B. Dangi, N. S. Leel, A. M. Quraishi, S. Z. Hashmi, S. Kumar, S. Dalela, J. Singh, B. L. Choudhary, M. A. Ahmad, P. A. Alvi, *Opt. Mater. (Amst).* **2024**, *148*, 114965.
[17] V. Dhayal, N. S. Leel, P. M. Z. Hasan, R. Darwesh, A. M. Quraishi, S. Z. Hashmi, S. Kumar, S. Dalela, J. Singh, P. A. Alvi, *Phys. Status Solidi Appl. Mater. Sci.* **2024**, *221*, 2300894.
[18] K. K. Khichar, S. B. Dangi, V. Dhayal, U. Kumar, S. Z. Hashmi, V. Sadhu, B. L. Choudhary, S. Kumar, S. Kaya, A. E. Kuznetsov, S. Dalela, S. K. Gupta, P. A. Alvi, *Polym. Compos.* **2020**, *41*, 2792–2802.
[19] Y. Chen, B. Song, M. Li, L. Lu, J. Xue, *Adv. Funct. Mater.* **2014**, *24*, 319–326.
[20] H. H. Li, Z. Y. Li, X. L. Wu, L. L. Zhang, C. Y. Fan, H. F. Wang, X. Y. Li, K. Wang, H. Z. Sun, J. P. Zhang, *J. Mater. Chem. A.* **2016**, *4*, 8242–8248.
[21] Y. Yu, C. H. Chen, J. L. Shui, S. Xie, *Angew. Chemie – Int. Ed.* **2005**, *44*, 7085–7089.
[22] S. Yasmeen, F. Iqbal, T. Munawar, M. A. Nawaz, M. Asghar, A. Hussain, *Ceram. Int.* **2019**, *45*, 17859–17873.
[23] L. Zhang, D. Ge, H. Geng, J. Zheng, X. Cao, H. Gu, *New J. Chem.* **2017**, *41*, 7102–7107.
[24] I. Gomaa, A. I. Abdel-Salam, A. Khalid, T. S. Soliman, *Opt. Laser Technol.* **2023**, *161*, 109126.
[25] S. M. Paek, E. J. Yoo, I. Honma, *Nano Lett.* **2009**, *9*, 72–75.
[26] K. Zhong, X. Xia, B. Zhang, H. Li, Z. Wang, L. Chen, *J. Power Sources.* **2010**, *195*, 3300–3308.
[27] N. F. Mahamad Yusoff, N. H. Idris, M. F. Md Din, S. R. Majid, N. A. Harun, L. Noerochim, *Nanomaterials* **2023**, *13*. https://doi.org/10.3390/nano13040732.
[28] T. S. Soliman, S. A. Vshivkov, A. I. Abdel-salam, I. Gomaa, A. Khalid, *Phys. Scr.* **2023**, *98*, 15832.
[29] C. C. Yang, Y. J. Lee, S. J. Chiu, K. T. Lee, W. C. Chien, C. T. Lin, C. A. Huang, *J. Appl. Electrochem.* **2008**, *38*, 1329–1337.

[30] R. Naeem, M. Ali Ehsan, R. Yahya, M. Sohail, H. Khaledi, M. Mazhar, *Dalt. Trans.* **2016**, *45*, 14928–14939.
[31] Y. F. Han, K. Ramesh, L. Chen, E. Widjaja, S. Chilukoti, F. Chen, *J. Phys. Chem. C.* **2007**, *111*, 2830–2833.
[32] H. R. Barai, A. N. Banerjee, N. Hamnabard, S. W. Joo, *RSC Adv.* **2016**, *6* 78887–78908.
[33] P. Gong, J. Xie, D. Fang, F. He, F. Li, K. Qi, *Mater. Res. Express.* **2017**, *4*, 0–8.
[34] S. B. Dangi, S. Z. Hashmi, U. Kumar, B. L. Choudhary, A. E. Kuznetsov, S. Dalela, S. Kumar, S. N. Dolia, S. Kumar, B. F. I. Sofi, R. Darwesh, P. M. Z. Hasan, P. A. Alvi, *Diam. Relat. Mater.* **2022**, *127*, 109158.
[35] A. I. Abdel-Salam, I. Gomaa, A. Khalid, T. S. Soliman, *Phys. Scr.* **2022**, *97*, 125807.
[36] S. I. Elkalashy, S. I. Khater, M. F. Zaki, *Polym. Eng. Sci.* **2024**, *64*, 4321–4331.
[37] S. Ayyaru, Y. Ahn, *J. Memb. Sci.* **2017**, *525*, 210–219.
[38] M. Sundaram, S. Abirami, D. Rana, N. Jacob, K. Divya, A. Nagendran, *J. Environ. Chem. Eng.* **2020**, *8*, 104426.
[39] E. M. Abdelrazek, I. S. Elashmawi, S. Labeeb, *Phys. B Condens. Matter.* **2010**, *405*, 2021–2027.
[40] E. Sheha, H. Khoder, T. S. Shanap, M. G. El-Shaarawy, M. K. El Mansy, *Optik (Stuttg)* **2012**, *123*, 1161–1166.
[41] J. Arya, N. S. Leel, Aakansha, A. M. Q., S. Z. Hashmi, S. Kumar, B. L. Choudhary, S. Dalela, Z. Hasan, J. Singh, P. A. Alvi, *Phys. Status Solidi Appl. Mater. Sci.* **2024**, *221*, 1–10.
[42] H. S. Jadhav, G. M. Thorat, B. B. Kale, J. G. Seo, *Dalt. Trans.* **2017**, *46*, 9777–9783.
[43] R. Gamal, E. Sheha, M. M. El Kholy, *RSC Adv.* **2023**, *13* 11959–11966.
[44] C. U. Devi, A. K. Sharma, V. V. R. N. Rao, *Mater. Lett.* **2002**, *56*, 167–174.
[45] A. K. Jonscher, *Thin Solid Films* **1967**, *1*, 213–234.
[46] A. R. Polu, R. Kumar, *Adv. Mater. Lett.* **2013**, *4*, 543–547.
[47] C. M. Kavitha, K. M. Eshwarappa, M. P. Shilpa, S. J. Shetty, S. Surabhi, A. P. Shashidhar, N. Karunakara, S. C. Gurumurthy, G. Sanjeev, *Mater. Res. Bull.* **2024**, *173*, 112685.
[48] M. H. Makled, E. Sheha, T. S. Shanap, M. K. El-Mansy, *J. Adv. Res.* **2013**, *4*, 531–538.

Manuscript received: August 08, 2024